

Holographic Aspects of Fermi Liquids in a Background Magnetic Field

Tameem Albash, Clifford V. Johnson

*Department of Physics and Astronomy
University of Southern California
Los Angeles, CA 90089-0484, U.S.A.*

talbash, johnson1, [at] usc.edu

Abstract

We study the effects of an external magnetic field on the properties of the quasiparticle spectrum of the class of 2+1 dimensional strongly coupled theories holographically dual to charged AdS_4 black holes at zero temperature. We uncover several interesting features. At certain values of the magnetic field, there are multiple quasiparticle peaks representing a novel level structure of the associated Fermi surfaces. Furthermore, increasing magnetic field deforms the dispersion characteristics of the quasiparticle peaks from non-Landau toward Landau behaviour. At a certain value of the magnetic field, just at the onset of Landau-like behaviour of the Fermi liquid, the quasiparticles and Fermi surface disappear.

1 Introduction

With increasing interest in the various long-anticipated potential applications to condensed matter and nuclear physics of gauge/gravity duality techniques such as AdS/CFT and its generalisations[1, 2, 3, 4], it has been of considerable interest to understand how to cleanly capture the physics of the Fermi surface of strongly coupled systems using holographic methods. This is because of the potential utility the methods might have to complement and extend the already impressive and ubiquitous power of the Fermi liquid paradigm, and also because there is a wealth of experimental phenomena that suggest that there are Fermi liquids that have behaviour that lies beyond the reach of standard techniques. Holographic methods may allow access to such behaviour.

Recently, the work of ref.[5] presented convincing evidence for the Fermi surface of the strongly interacting 2+1 dimensional system at zero temperature and finite density that is holographically dual[6, 7] to an extremal electrically charged Reissner–Nordström black hole in four dimensional anti-de Sitter spacetime (AdS_4). (That work continued and refined the important initial studies presented in ref.[8], and there has been further discussion and extension of this particular line of development in refs.[9, 10]. See also ref.[11] for a discussion of possible holographic descriptions of Fermi surfaces in a different context.)

A key observation of ref.[5] was the fact that the Fermi liquid had distinctly non-Landau behaviour, showing unusual dispersion characteristics of the quasiparticle peak. This is perhaps to be expected, not just because the system is strongly coupled (remember that Landau Fermi-liquids arise in strongly coupled contexts too), but because one might anticipate that the effectively weakly coupled quasiparticle theory that arises (after strong coupling dressing) in the vicinity of the Fermi surface ought not to have a (simple) gravitational dual. When all is said and done, it is, after all, just a free field theory¹. One might wonder, however, what range of dispersion characteristics might be accessible using holographic duals, and in particular how close one can get to Landau-like behaviour for a given system. The recent work of ref.[10] answers some of this by doing a careful analysis of the $\text{AdS}_2 \times \mathbb{R}^2$ throat region region (first discussed in this holographic context in ref.[6]) that appears near the horizon of the black hole at zero temperature. Much of the physics of the critical exponents can be traced to the IR physics located down this throat and is controlled by the masses of fields there.

Our work shows a different way of deforming the critical behaviour. As we will show,

¹See, however, the work of ref.[9], but study it alongside the discussion in section VI.E. of ref.[10].

adding a magnetic field moves the dispersion of the quasiparticle spectrum back *toward* Landau-like behaviour, in a manner that may have precise experimental analogues, especially given how natural magnetic fields are as laboratory probes and control parameters in a condensed matter context. Moreover, we find that at a given value of the magnetic field \mathcal{H} (below what appears to be a certain limiting value \mathcal{H}_{\max}), multiple quasiparticle peaks can appear in the spectrum, representing a *finite* series of levels (a kind of “band” structure). Our boundary condition is such that we are at the zeroth Landau level, so the levels we see are not the infinite family of equally spaced Landau–Rabi levels known from weak coupling intuition.

To introduce a background magnetic field \mathcal{H} we simply add magnetic charge to the AdS₄–RN black hole, making it a dyon. We then study the system by probing it (as done in the $\mathcal{H} = 0$ case) with a minimally coupled Dirac fermion of electric charge q . We compute the retarded Green’s function associated with this probe, from which, after Fourier transforming to momentum–frequency space (k, w) , we extract our physics.

Generically, it can be seen that the magnetic field shifts the effective mass of the fermion, which translates into a deformation of effective dimension of the operator we are probing the theory with. Following the discussion in refs.[9, 10], it is not hard to infer that this will certainly affect the dispersion of the resulting quasiparticle peaks, but this needs to be explored explicitly, and this is what we report on in this paper.

2 Background

The metric for the dyonic black hole in asymptotically AdS₄ spacetime, using Cartesian coordinates is[12]:

$$\begin{aligned}
 ds^2 &= \frac{L^2 \alpha^2}{z^2} (-f(z) dt^2 + dx^2 + dy^2) + \frac{L^2}{z^2} \frac{dz^2}{f(z)} , \\
 F &= 2H\alpha^2 dx \wedge dy + 2Q\alpha dz \wedge dt , \\
 f(z) &= 1 + (H^2 + Q^2) z^4 - (1 + H^2 + Q^2) z^3 = (1 - z) (z^2 + z + 1 - (H^2 + Q^2) z^3) .
 \end{aligned} \tag{1}$$

Here L is the length scale set by the negative cosmological constant $\Lambda = -3/L^2$ in Einstein–Maxwell theory given by:

$$S_{\text{bulk}} = \frac{1}{2\kappa_4^2} \int d^4x \sqrt{-G} \left\{ R + \frac{6}{L^2} - \frac{L^2}{4} F^2 \right\} , \tag{2}$$

where $\kappa_4^2 = 8\pi G_N$ is the gravitational coupling and our signature is $(-+++)$. The mass per unit volume and temperature of the black hole are:

$$\varepsilon = \frac{\alpha^3 L^2}{\kappa_4^2} [1 + Q^2 + H^2] , \quad T = \frac{\alpha}{4\pi} [3 - (Q^2 + H^2)] . \quad (3)$$

These are also the energy density and temperature of the 2+1 dual theory, which can be roughly thought of as living on the boundary at $z = 0$. The horizon of the hole is at $z = 1$. We choose our gauge such that the gauge field can be written in the following form:

$$A_t = 2Q\alpha(z - 1) , \quad A_x = -2H\alpha^2 y . \quad (4)$$

The electric component sets, by virtue of its value on the boundary, a chemical potential $\mu = -2Q\alpha$ for the $U(1)$ charge, while the magnetic component determines a background magnetic field of magnitude $\mathcal{H} = -2H\alpha^2$. The parameter α has dimensions of inverse length. For simplicity, in the sequel we make the following redefinitions so that we are working entirely in terms of dimensionless fields and coordinates:

$$t \rightarrow t/\alpha , \quad x \rightarrow x/\alpha , \quad y \rightarrow y/\alpha , \quad A_t \rightarrow \alpha A_t . \quad (5)$$

2.1 The Probe Fermion

We consider the Dirac action in this background:

$$S_D = \int d^4x \sqrt{-G} i (\bar{\Psi} \Gamma^M \mathcal{D}_M \Psi - m \bar{\Psi} \Psi) , \quad (6)$$

where \mathcal{D}_M is the covariant derivative given by:

$$\mathcal{D}_M = \partial_M + \frac{1}{4} \omega_{abM} \Gamma^{ab} - iq A_M , \quad (7)$$

and M are world indices and a, b are tangent-space indices. ω_{abM} is the spin connection given by:

$$\omega_{abM} = e_a^N \partial_M e_{bN} - e_{aN} e_b^O \Gamma_{OM}^N , \quad (8)$$

and

$$\Gamma^{ab} = \frac{1}{2} [\Gamma^a, \Gamma^b] , \quad \Gamma^M = e_a^M \Gamma^a . \quad (9)$$

The Dirac equation is given by:

$$\Gamma^M \mathcal{D}_M \Psi - m \Psi = 0 . \quad (10)$$

We choose Ψ such that:

$$\Psi = z^{3/2} f^{-1/4} e^{-i\omega t + k_x x} \begin{pmatrix} \phi_+(y, z) \\ \phi_-(y, z) \end{pmatrix}, \quad (11)$$

and

$$\Gamma^3 = \begin{pmatrix} 1 & 0 \\ 0 & -1 \end{pmatrix}, \quad \Gamma^\mu = \begin{pmatrix} 0 & \gamma^\mu \\ \gamma^\mu & 0 \end{pmatrix}. \quad (12)$$

This reduces the equation of motion to:

$$\sqrt{\frac{g_{xx}}{g_{zz}}} (\partial_z \mp m\sqrt{g_{zz}}) \phi_\pm = \pm i (\gamma^0 u + i\gamma^2 \partial_y - \gamma^1 (2Hqy + k_x)) \phi_\mp \quad (13)$$

where:

$$u = \sqrt{\frac{g_{xx}}{-g_{tt}}} (\omega + 2qQ(z-1)), \quad \sqrt{\frac{g_{xx}}{g_{zz}}} = \sqrt{f}, \quad \sqrt{\frac{g_{xx}}{-g_{tt}}} = \frac{1}{\sqrt{f}}. \quad (14)$$

Consider the limit of $z \rightarrow 0$ of this equation. The solution is given by:

$$\phi_+ = Az^m + z^{1-m} \frac{i(\gamma^0 u - \gamma^1 (2Hqy + k_x) + i\gamma^2 \partial_y)}{1 - 2m} B, \quad (15)$$

$$\phi_- = Bz^{-m} + z^{m+1} \frac{-i(\gamma^0 u + \gamma^1 (2Hqy + k_x) - i\gamma^2 \partial_y)}{1 + 2m} A, \quad (16)$$

where A and B are functions independent of z . The various relationships between the various powers of z is relevant for the AdS/CFT dictionary [13]. In particular, if we restrict ourselves to $m \geq 0$, then the source of the dual operator is proportional to B , and the vacuum expectation value (vev) of the operator is proportional to A . In this case, the dimension of the operator is given by:

$$\Delta = \frac{d}{2} + m. \quad (17)$$

We now proceed away from $z = 0$ and further decompose the two-component fields ϕ_\pm as:

$$\phi_\pm = \begin{pmatrix} \chi_\pm \\ \xi_\pm \end{pmatrix}, \quad (18)$$

and make the following choices for the γ 's:

$$\gamma^0 = i\sigma_2, \quad \gamma^1 = \sigma_1, \quad \gamma^2 = \sigma_3, \quad (19)$$

and these fields satisfy the following coupled equations of motion

$$\sqrt{\frac{g_{xx}}{g_{zz}}} (\partial_z \mp m\sqrt{g_{zz}}) \chi_\pm = \mp [-iu\xi_\mp + \partial_y \chi_\mp + i(2Hqy + k_x) \xi_\mp], \quad (20)$$

$$\sqrt{\frac{g_{xx}}{g_{zz}}} (\partial_z \mp m\sqrt{g_{zz}}) \xi_\pm = \mp [iu\chi_\mp - \partial_y \xi_\mp + i(2Hqy + k_x) \chi_\mp]. \quad (21)$$

3 Specializations

3.1 Zero Temperature

Henceforth we will work at zero temperature. This means, from equation (3) that there is a relation between Q and H that we must bear in mind:

$$Q = (3 - H^2)^{\frac{1}{2}} . \quad (22)$$

In particular, note that (we temporarily restore α for this discussion) the chemical potential $\mu = -2\alpha Q$ naively gets shifted from its ($T = 0, H = 0$) value due to this relation. Also of note is the fact that as H increases, Q must decrease in order to keep the temperature vanishing. There is a maximum value of H , $H_{\max} = \sqrt{3}$, at which Q vanishes. This is all to be physically interpreted for our system as follows. First, we need to decide what physical quantity we are holding fixed while adding magnetic field to the system. A good such quantity is the chemical potential $\mu = -2\alpha Q$. Even though Q decreases for non-zero H , we simply increase α to hold it at the same value that it was at zero H . (According to equation (3), this increases the energy density ε of the field theory, but this is quite natural as the magnetic field lifts the available energy levels of all charged particles.) Writing $3 - H^2 = \tilde{Q}^2 \delta^2$ we can write $\alpha = \tilde{\alpha} \delta^{-1}$ so that μ is fixed as $\delta \rightarrow 0$. Meanwhile we see that the physical magnetic field $\mathcal{H} = -2\alpha^2 H$ goes to infinity, showing that we do not have a limiting *physical* applied magnetic field.

3.2 A Zero Temperature Ansatz

In order to satisfy the appropriate boundary conditions at the event horizon, we redefine the fields as follows (for $\omega \neq 0$; see subsection 3.4 for a comment on the $\omega = 0$ case):

$$\begin{aligned} \chi_{\pm} &= a_{\pm}(y, z) \exp\left(\frac{i\omega}{6(1-z)}\right) (1-z)^{i(6qQ-4\omega)/18} , \\ \xi_{\pm} &= b_{\pm}(y, z) \exp\left(\frac{i\omega}{6(1-z)}\right) (1-z)^{i(6qQ-4\omega)/18} . \end{aligned} \quad (23)$$

With this field redefinition, the equations of motion expanded at the event horizon give the following conditions:

$$a_+(y, 1) = b_-(y, 1) , \quad a_-(y, 1) = -b_+(y, 1) , \quad (24)$$

This result suggests that the ‘‘correct’’ variables to study the problem are actually:

$$A_+(y, z) = b_-(y, z) - a_+(y, z) , \quad A_-(y, z) = -i(a_-(y, z) + b_+(y, z)) , \quad (25)$$

$$B_+(y, z) = a_+(y, z) + b_-(y, z) , \quad B_-(y, z) = i (b_+(y, z) - a_-(y, z)) . \quad (26)$$

The equations of motion are now given by:

$$\begin{aligned} \sqrt{\frac{g_{xx}}{g_{zz}}} \left(\partial_z + \frac{i\omega}{6(1-z)^2} + i \frac{-6qQ + 4\omega}{18(1-z)} \right) A_+ = \\ - \sqrt{g_{xx}} m B_+ - i u A_+ + i (\partial_y B_- + (2Hqy + k_x) B_+) , \end{aligned} \quad (27)$$

$$\begin{aligned} \sqrt{\frac{g_{xx}}{g_{zz}}} \left(\partial_z + \frac{i\omega}{6(1-z)^2} + i \frac{-6qQ + 4\omega}{18(1-z)} \right) A_- = \\ - \sqrt{g_{xx}} m B_- - i u A_- - i (\partial_y B_+ + (2Hqy + k_x) B_-) , \end{aligned} \quad (28)$$

$$\begin{aligned} \sqrt{\frac{g_{xx}}{g_{zz}}} \left(\partial_z + \frac{i\omega}{6(1-z)^2} + i \frac{-6qQ + 4\omega}{18(1-z)} \right) B_+ = \\ - \sqrt{g_{xx}} m A_+ + i u B_+ - i (\partial_y A_- + (2Hqy + k_x) A_+) , \end{aligned} \quad (29)$$

$$\begin{aligned} \sqrt{\frac{g_{xx}}{g_{zz}}} \left(\partial_z + \frac{i\omega}{6(1-z)^2} + i \frac{-6qQ + 4\omega}{18(1-z)} \right) B_- = \\ - \sqrt{g_{xx}} m A_- + i u B_- + i (\partial_y A_+ + (2Hqx + k_x) A_-) . \end{aligned} \quad (30)$$

At the event horizon, we impose the following condition:

$$\partial_y B_{\pm}(y, 1) + 2Hqy B_{\mp}(x, 1) = 0 , \quad (31)$$

which has solution given by:

$$\begin{aligned} B_+(y, 1) = B_-(y, 1) = B_0 \exp(-Hqy^2) , \\ B_+(y, 1) = -B_-(y, 1) = B_0 \exp(Hqy^2) , \end{aligned} \quad (32)$$

This solution can be understood as an infinite sum of the separable solutions of the problem in terms of the coordinate $\eta = \sqrt{2Hq}(y + k_x/2Hq)$. For this reason, we refer to this solution as the ‘‘infinite-sum’’ solution. We elaborate more on this relationship in our companion paper [14]. This boundary condition restricts us to the zeroth Landau level. This then leaves us with the following conditions at the event horizon:

$$A_{\pm}(r, 1) = 0 , \quad \partial_z A_{\pm}(r, 1) = \mp \frac{\sqrt{6}}{2\omega} (k_x \pm im) B_{\pm} , \quad (33)$$

$$\begin{aligned} \partial_z B_{\pm}(x, 1) &= -\frac{i}{108} \left((48qQ - 23\omega) B_{\pm} \mp 18\sqrt{6} (k_x \mp im) \partial_z A_{\pm}(x, 1) \right. \\ &\quad \left. \mp 18\sqrt{6} \partial_z (\partial_y A_{\mp} + 2Hqy A_{\pm}) \right) , \\ &= -\frac{i}{108} \left(48qQ - 23\omega + \frac{54}{\omega} (k_x^2 + m^2 + 4Hqy (k_x \mp im)) \right) B_0 . \end{aligned} \quad (34)$$

Which solution is chosen depends on the direction of the magnetic field. For the rest of our analysis, we stick to the solution with $B_+ = B_-$ which means we have negative H .

In all that follows, we restrict ourselves to $m = 0$ for our probe fermion. By the AdS/CFT dictionary, this means we are turning on operators with dimension $\Delta = 3/2$. This case was studied in great detail for the case of $H = 0$ in ref. [5].

3.3 Extracting the retarded Green's function

Following the prescription for extracting the Green's function from ref. [13], the Green's function is given by (assuming $m \geq 0$):

$$G_R = \lim_{\epsilon \rightarrow 0} \epsilon^{-2m} \begin{pmatrix} i \frac{\chi_+(k)}{\xi_-(k)} & 0 \\ 0 & -i \frac{\xi_+(k)}{\chi_-(k)} \end{pmatrix}, \quad (35)$$

which in term of our fields A_\pm and B_\pm gives:

$$G_+ = i \frac{\chi_+(k)}{\xi_-(k)} = i \frac{B_+(k) - A_+(k)}{B_+(k) + A_+(k)} \quad G_- = -i \frac{\xi_+(k)}{\chi_-(k)} = i \frac{B_-(k) - A_-(k)}{B_-(k) + A_-(k)}. \quad (36)$$

Note that these fields are given in momentum-space and not position-space. A subtlety here is that in ref. [13], the fields always had a separable form with respect to the AdS radial coordinate and the space-time coordinates of the field theory, whereas here this is not the case. We assume that the prescription continues to hold and we simply Fourier transform our fields at the AdS boundary and use the result in the prescription.

3.4 The case of $\omega = 0$.

For the special case of $\omega = 0$, the condition $A_\pm(y, 1) = 0$ is no longer required. In fact, we need to change the behavior of the fields at the event horizon. Consider first the $H = 0$ case. We go back to equations (23) and make the following redefinition:

$$\chi_\pm(z) = a_\pm(z) (1-z)^{\frac{\sqrt{2}}{6} \sqrt{3k^2 - 2q^2 Q^2}}, \quad (37)$$

$$\xi_\pm(z) = b_\pm(z) (1-z)^{\frac{\sqrt{2}}{6} \sqrt{3k^2 - 2q^2 Q^2}}. \quad (38)$$

The exponent of the $(1-z)$ term is chosen such that there is a non-zero solution for the fields. Now we define A_\pm and B_\pm as before, and find the following condition at the event horizon:

$$A_+(1) = -\frac{1}{\sqrt{6}k} \left(2qQ + i\sqrt{2}\sqrt{3k^2 - 2q^2 Q^2} \right) B_+(1), \quad (39)$$

$$A_-(1) = \frac{1}{\sqrt{6}k} \left(2qQ + i\sqrt{2}\sqrt{3k^2 - 2q^2 Q^2} \right) B_-(1). \quad (40)$$

In particular, if we take $B_+(1) = B_-(1)$, we have $A_-(1) = -A_+(1)$, and we get for our Green's functions at the event horizon:

$$G_+ = -\frac{\sqrt{3k^2 - 2q^2Q^2}}{\sqrt{3k} - \sqrt{2qQ}}, \quad G_- = \frac{\sqrt{3k^2 - 2q^2Q^2}}{\sqrt{3k} + \sqrt{2qQ}}. \quad (41)$$

Another independent solution is to take:

$$\chi_{\pm}(z) = a_{\pm}(z) (1-z)^{-\frac{\sqrt{2}}{6} \sqrt{3k^2 - 2q^2Q^2}}, \quad (42)$$

$$\xi_{\pm}(z) = b_{\pm}(z) (1-z)^{-\frac{\sqrt{2}}{6} \sqrt{3k^2 - 2q^2Q^2}}, \quad (43)$$

which gives at the event horizon:

$$A_+(1) = -\frac{1}{\sqrt{6k}} \left(2qQ - i\sqrt{2} \sqrt{3k^2 - 2q^2Q^2} \right) B_+(1), \quad (44)$$

$$A_-(1) = \frac{1}{\sqrt{6k}} \left(2qQ - i\sqrt{2} \sqrt{3k^2 - 2q^2Q^2} \right) B_-(1). \quad (45)$$

Again if we take $B_+(1) = B_-(1)$, we have $A_-(1) = -A_+(1)$ but with the Green's function gives as:

$$G_+ = \frac{\sqrt{3k^2 - 2q^2Q^2}}{\sqrt{3k} - \sqrt{2qQ}}, \quad G_- = -\frac{\sqrt{3k^2 - 2q^2Q^2}}{\sqrt{3k} + \sqrt{2qQ}}. \quad (46)$$

If we now turn on H , the situation becomes much more complicated. The equations of motion for A_{\pm} and B_{\pm} at the horizon require a more complicated exponent for $(1-z)$ in their behaviour. For our purposes, we will have no need to focus on the case of $\omega = 0$ and determine these exponents since the interesting physics (specifically, the quasiparticle peaks) will appear away from $\omega = 0$. We will therefore not pursue this further in the present work.

4 Solutions

4.1 A Separable Solution

Recalling that we will work with $m = 0$ henceforth, we begin by considering the trivial case of a separable solution which occurs for $k_x = 0$, *i.e.*

$$A_{\pm}(y, z) = A(z) \exp(-Hqy^2), \quad B_{\pm}(y, z) = B(z) \exp(-Hqy^2). \quad (47)$$

In this case, the four equations of motion reduce to two:

$$\sqrt{\frac{g_{xx}}{g_{zz}}} \left(\partial_z A + \frac{i\omega}{6(1-z)^2} A + i \frac{-6qQ + 4\omega}{18(1-z)} A \right) = -iuA, \quad (48)$$

$$\sqrt{\frac{g_{xx}}{g_{zz}}} \left(\partial_z B + \frac{i\omega}{6(1-z)^2} B + i \frac{-6qQ + 4\omega}{18(1-z)} B \right) = iuB. \quad (49)$$

Therefore in the separable case, $G_R(1, 1) = G_R(2, 2)$. In fact, looking at the initial conditions at the event horizon for $A(z)$, we find that $\partial_z A(1) = A(1) = 0$, and therefore we can consistently take $A(z) = 1$. Therefore, we automatically get that $G_R(1, 1) = i$.

The other separable solution occurs for $H = 0$, and our solution should match those of ref. [5]. In this case, we can take:

$$A_{\pm}(y, z) = A_{\pm}(z) , \quad B_{\pm}(y, z) = B_{\pm}(z) . \quad (50)$$

Choosing $q = -0.5$ we do indeed recover the results of ref. [5], as we show in figure 1. These two cases of separable solutions provide good test cases for the accuracy of numerical

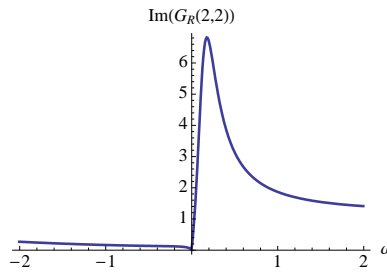


Figure 1: Solution for $H = 0$ and $k_x = 1.2$ using Mathematica’s NDSolve

procedure when we solve the infinite–sum cases next.

Before proceeding, we emphasize that our separable ansatz in equation (47) only considers the zeroth order Hermite function. The ansatz can be generalized for higher order Hermite functions, the physics of which we study in a companion paper [14].

4.2 Infinite–sum cases: Full Numerical Method

We now proceed to solve the problem with $k \neq 0$ and $H \neq 0$. We choose to discretize the equations of motion using a “fully–implicit” method:

$$A_+(y_j, z_n) = A_+(y_j, z_{n-1}) - i\Delta z F_+(z_{n-1}) A_+(y_j, z_{n-1}) + i \frac{\Delta z}{\sqrt{f(z_{n-1})}} \left(\frac{B_-(y_{j+1}, z_{n-1}) - B_-(y_{j-1}, z_{n-1})}{2\Delta y} + (2Hqy_j + k_x) B_+(y_j, z_{n-1}) \right) , \quad (51)$$

where we have defined:

$$F_+(z) = \frac{\omega}{6(1-z)^2} + \frac{-6qQ + 4\omega}{18(1-z)} + \frac{u}{\sqrt{f(z)}} . \quad (52)$$

The problem is now to solve a large number of linear equations at each z step. The associated matrix is of block tri-diagonal form, i.e. :

$$\begin{pmatrix} \ddots & & & & & & & \\ \cdots & A_1 & B_1 & C_1 & 0 & 0 & \cdots & \\ \cdots & 0 & A_2 & B_2 & C_2 & 0 & \cdots & \\ \cdots & 0 & 0 & A_3 & B_3 & C_3 & \cdots & \\ & & & & & & & \ddots \end{pmatrix}, \quad (53)$$

where each of the A_i, B_i, C_i 's are matrices (8×8 matrices in this case). This matrix can be inverted using a “forward elimination–backward substitution” method.

4.2.1 Accuracy of Numerics: Two Tests

The first test of our numerical method is to reproduce the known separable results we describe above. We present the result for $H = 0$, (with $k_y = 0$ and non-zero k_x) in figures 2 and 3, demonstrating with the latter that we can reproduce the correct quasiparticle peak and its associate scaling behaviour. It is interesting to test the case of $k_x = 0$.

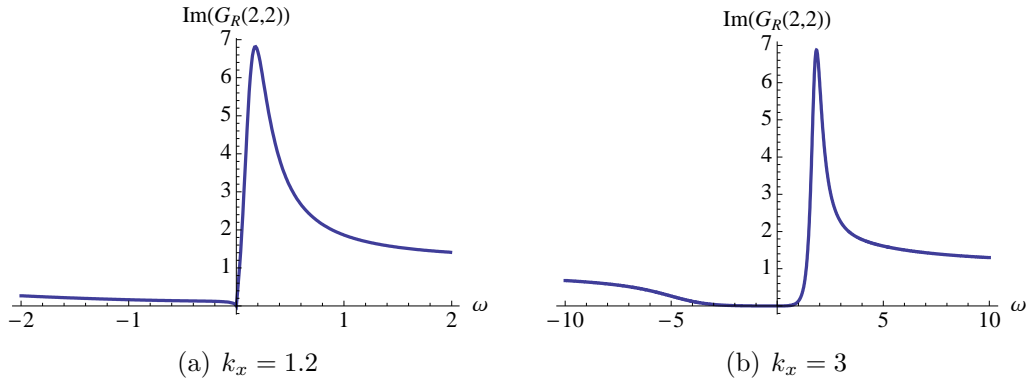


Figure 2: Solution for $H = 0$ using implicit method to solve PDE.

We find considerable deviation from the expected answer of $G_R(2,2) = i$. We can understand this completely as arising from numerical error. The field A_+ at the boundary should be zero in this case, but it turns out to be proportional to the derivative of the B 's. It is straight-forward to understand this discrepancy: it comes from the finite difference approximation to the y -derivative, which has zeros for non-zero H at zero k_x , causing a loss of accuracy. Given that we have rotational symmetry, we can choose, without loss of generality, to put all our momentum into k_x and work in the more well-behaved $k_y = 0$ sector for the remainder of our investigations.

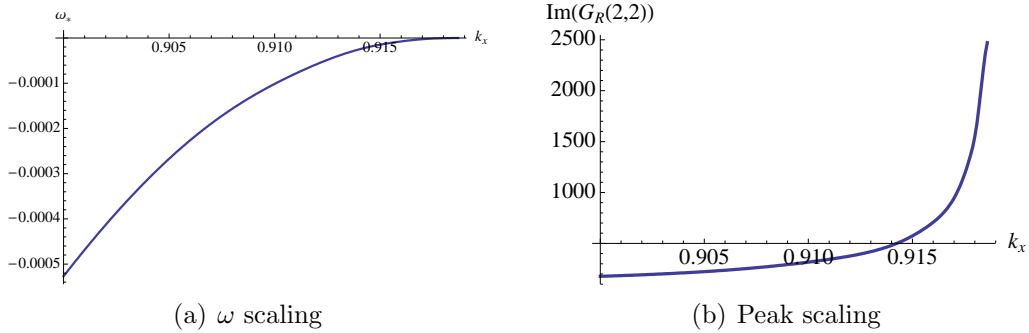


Figure 3: Scaling behavior of ω^* (location) and the height of the peak near the pole at $\omega = 0$ and $k_x \approx 0.918$.

We are now ready to numerically explore (k, ω) landscape for various H , searching for quasiparticle poles in the Green's function.

5 Observations

There are several important general features that we encountered in our numerical explorations, and we collect them all together here.

5.1 A Gap, A Ridge, and Some Poles

- For a given magnetic field, as k_x is increased, a region appears where $\text{Im}(G_R(2,2))$ is negative for values of $\omega < \omega_{\text{gap}}$. We explain the meaning of this region below, but we illustrate in figure 4 how ω_{gap} behaves as we increase k_x for fixed magnetic field. In particular, we note that as $k_x \rightarrow \infty$, the behavior of ω_{gap} is linear and appears to remain a fixed distance from the $\omega = k_x$ line. For higher magnetic fields, the separation from the line decreases.
- We find a peak for values of $\omega > \omega_{\text{gap}}$. We refer to the position of the peak as ω_* . We show samples of the behavior of ω_* in figure 5. This is the ridge of ref. [5]. From figure 5, one sees that as the magnetic field is increased, the ridge gets closer to the $\omega = k_x$ line, crosses it, and continues to approach it from above (see figure 5(b)). In addition, the ridge always remains above the gap line (except when they meet). We show this in figure 6. We also show an example of the large k_x behavior for different magnetic fields in figure 7.

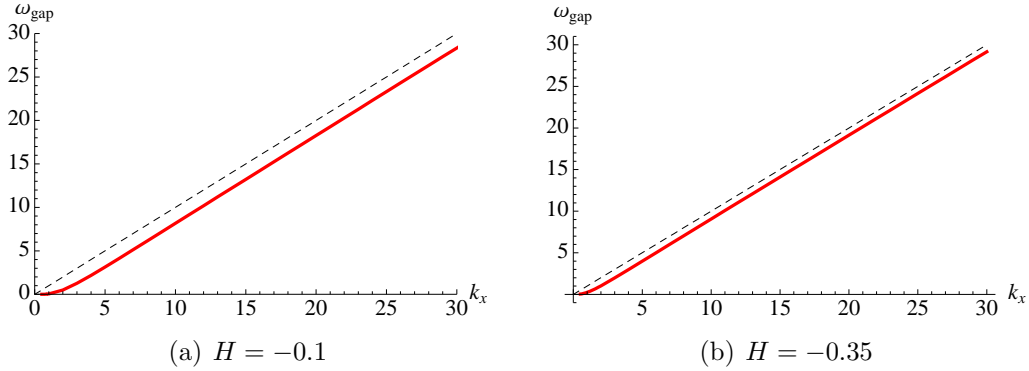


Figure 4: Position of the edge of the gap for fixed H as k_x is increased. The dashed line is the line of $\omega = k_x$.

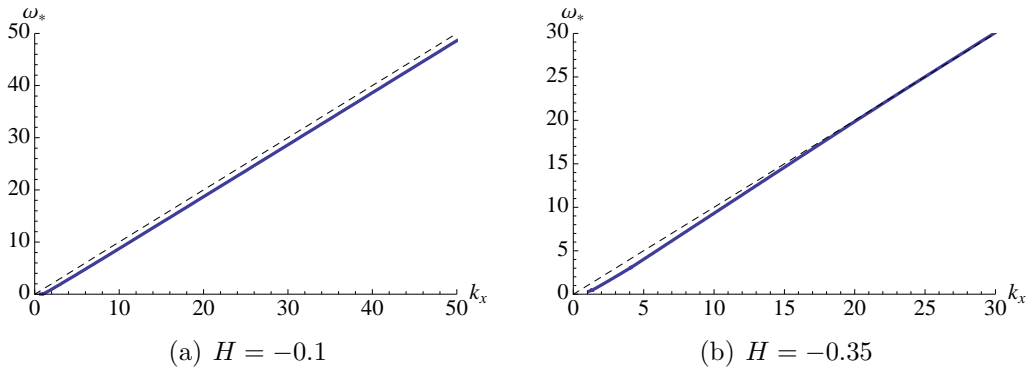


Figure 5: Position of the peak for fixed H as k_x is increased. The dashed line is the line of $\omega = k_x$.

- For a fixed value of H , when $\omega_{\text{gap}} = \omega_*$ at some $k_x = k_F$, we find a pole in $\text{Im}G_R(2, 2)$. Notice that this means that a pole appears whenever the ridge curve touches the gap curve. We find that the curves never cross but bounce off each other. We show an example of such a pole in figure 8. This is a quasiparticle peak. It indicates a Fermi surface at k_F . Away from the poles, the numerical results should be interpreted carefully since there one should consider a complex ω and not a purely real ω . This is relevant because in our numerics the poles occur immediately after a region where the imaginary part of the Green function is negative, which is not allowed if the theory is unitary. We believe that the proper treatment of the complex ω in these regions would resolve this.

The fact that $\omega > 0$ tells us that the Fermi energy E_F is greater than the $U(1)$ chemical

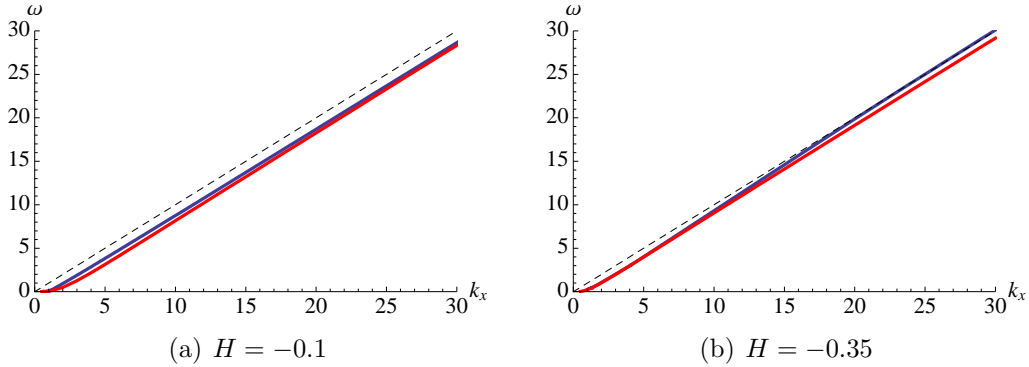


Figure 6: Position of the peak and gap for fixed H as k_x is increased. The dashed line is the line of $\omega = k_x$.

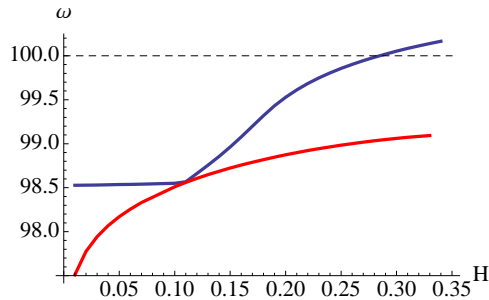


Figure 7: Behavior of ω_{gap} (red) and ω_* (blue) at fixed $k_x = 100$

potential μ . This is quite natural: the physical magnetic field $\mathcal{H} = -2\alpha^2 H$ has lifted the energy of the charged particle, as earlier discussed. (Note that we see peaks for negative ω as well, but focus on positive ω for physical interpretation.)

In particular, we note that the behavior is very reminiscent of the behavior of the full Green's function (that includes both the advanced and retarded Green's function) at the Fermi surface where both quasiparticles and quasiholes are observed. It is also important to note that there can be multiple (but we believe only a finite number) such peaks, at a given H , appearing at distinct values (ω_*, k_x) .

- There exists a maximum magnitude of the magnetic field at approximately $|H| \gtrsim 0.37$ above which we do not find any poles. We notice that above this maximum, the ridge remains above the $w = k_x$ line for all values of k_x and the gap remains below the line, preventing the two from meeting. We explain in the following subsection what this maximum corresponds to.

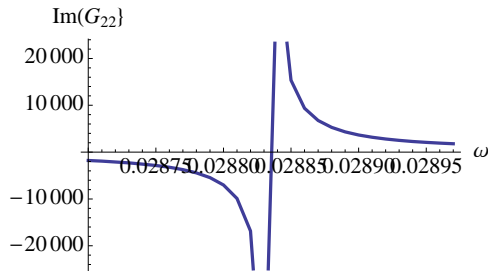


Figure 8: Behavior of the pole in the $\text{Im}G_R(2, 2)$ for $H = -0.1$ at $k_x = 0.871847$

5.2 Dispersion of the Quasiparticle Peaks

We proceed to study the scaling properties of the poles observed in $\text{Im}(G_R(2, 2))$. We present samples of the results in figure 9. We find that the behavior near the pole seems very close to linear once $H \neq 0$, if approaching from below or above. Contrast this with the case of $H = 0$ (discovered in ref.[5], recomputed here and displayed in figure 3). However, as one can see from the figure, there is always a change in slope as we go from $k < k_F$ to $k > k_F$. This suggests that there is perhaps curvature to the lines infinitesimally close to k_F . Therefore, the system is still in a non-Landau Fermi liquid regime but with a scaling less than that found for the $H = 0$ case.

Crucially, we see that as we increase the magnetic field, the slopes of the two lines begin to approach each other. Our results suggest that when the slopes approach the limit of being equal, that is exactly when we no longer find any poles. This seems to be the mechanism by which the system protects itself from becoming a simple (linear) Landau Fermi liquid, as discussed in the introduction.

In addition, we note that when there are multiple poles present (for a given H), the dispersion behavior of the poles may not be the same. We present an example of this in figure 10. The results suggest that the further along the ridge one finds a pole, the more the behavior of the pole approaches that of a Landau Fermi liquid (*i.e.*, linear dispersion). This suggests why there may only be a finite number of poles for a fixed magnetic field, since as we saw earlier, beyond a certain H , or far enough along the ridge, the ridge and gap no longer cross.

6 Conclusions

We've found a rich set of physical results (the deformation of dispersion characteristics, and the discrete Fermi levels) from our holographic studies of the Fermi surface and quasiparticle

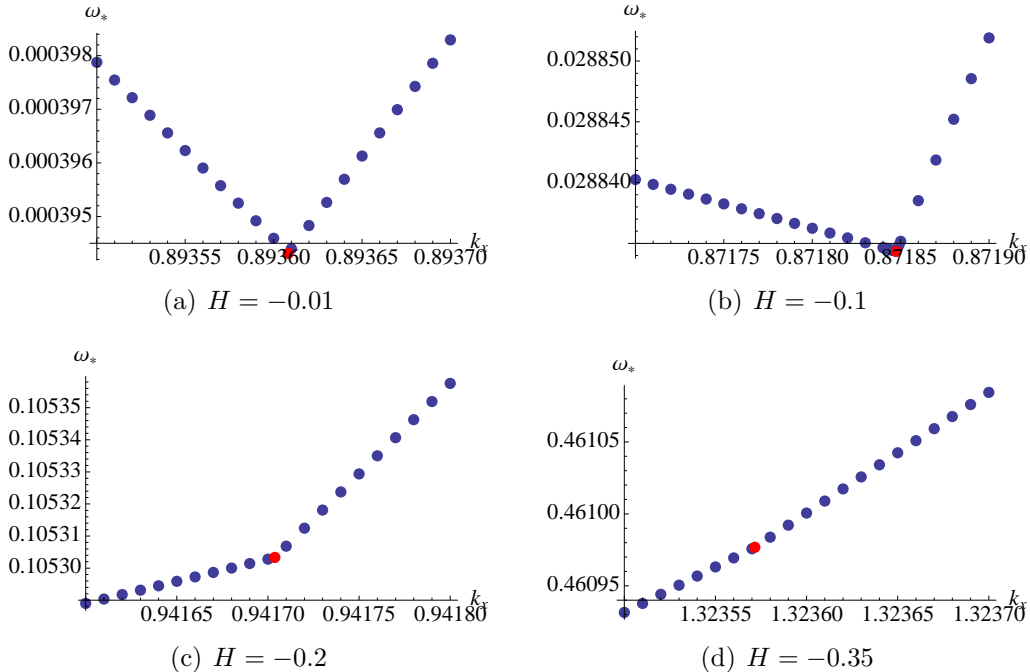


Figure 9: Scaling behavior of ω_* . The red dot is where the pole is located, which corresponds to where the two lines intersect.

spectrum in a background magnetic field. We expect that there is even more rich physics to be found from these systems. It is very exciting that some of these phenomena seem akin to the sorts of strongly coupled physics that are experimentally accessible, including with background magnetic fields as a probe of physics.

Our exploration work was primarily numerical. A precise analytic relation between the value of the magnetic field and the nature of the dispersion of the peaks would be a valuable result. However, there is an apparent obstruction to doing the obvious generalization of the analysis of ref.[10] that exploits the presence of the $\text{AdS}_2 \times \mathbb{R}^2$ region. There, an expansion about the $\omega = 0$ point, where the quasiparticle peak appears, representing a Fermi surface with Fermi energy E_F equal to the $U(1)$ chemical potential μ .

Things are different in our case. While it is trivial to show that there is again an $\text{AdS}_2 \times \mathbb{R}^2$ region near the horizon of the dyon (rather nicely, the electric field is entirely in the AdS_2 and the magnetic field is entirely threading the \mathbb{R}^2), this is not enough. In the presence of magnetic field, the energy of the system gets lifted. The lowest available level at which we find a quasiparticle peak, for a given \mathcal{H} has Fermi energy E_F greater than the $U(1)$ chemical potential μ , and so occurs away from the $\omega = 0$ point that was the focus of

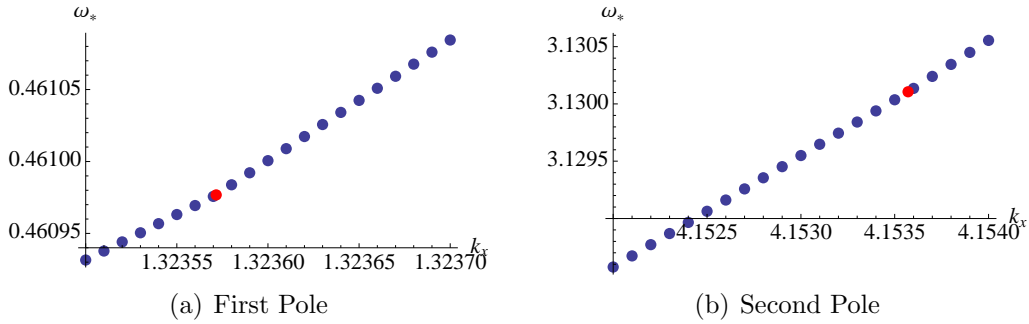


Figure 10: Scaling behavior of ω_* for two poles at fixed magnetic field $H = -0.35$. The red dot is where the pole is located, which corresponds to the two lines intersect.

refs.[5, 10]. There is no good analytical guide (so far) as to where in ω the peaks will arise, and so we search for them numerically. An analytical characterization of exactly how the presence of \mathcal{H} affects the dispersion relation will have to await future work.

Acknowledgments

We would like to thank Arnab Kundu and Mohammad Edalati for conversations that led to this project. CVJ thanks Ruth Andrew Ellenson for an insightful remark and the Aspen Center for Physics for a stimulating working atmosphere while some of this work was carried out. This work was supported by the US Department of Energy.

References

- [1] J. M. Maldacena, “The large N limit of superconformal field theories and supergravity,” *Adv. Theor. Math. Phys.* **2** (1998) 231–252, [hep-th/9711200](#).
- [2] E. Witten, “Anti-de Sitter space and holography,” *Adv. Theor. Math. Phys.* **2** (1998) 253–291, [hep-th/9802150](#).
- [3] S. S. Gubser, I. R. Klebanov, and A. M. Polyakov, “Gauge theory correlators from non-critical string theory,” *Phys. Lett.* **B428** (1998) 105–114, [hep-th/9802109](#).
- [4] E. Witten, “Anti-de Sitter space, thermal phase transition, and confinement in gauge theories,” *Adv. Theor. Math. Phys.* **2** (1998) 505–532, [hep-th/9803131](#).
- [5] H. Liu, J. McGreevy, and D. Vegh, “Non-Fermi liquids from holography,” [0903.2477](#).

- [6] A. Chamblin, R. Emparan, C. V. Johnson, and R. C. Myers, “Charged AdS black holes and catastrophic holography,” *Phys. Rev.* **D60** (1999) 064018, [hep-th/9902170](#).
- [7] A. Chamblin, R. Emparan, C. V. Johnson, and R. C. Myers, “Holography, thermodynamics and fluctuations of charged AdS black holes,” *Phys. Rev.* **D60** (1999) 104026, [hep-th/9904197](#).
- [8] S.-S. Lee, “A Non-Fermi Liquid from a Charged Black Hole: A Critical Fermi Ball,” *Phys. Rev.* **D79** (2009) 086006, [0809.3402](#).
- [9] M. Cubrovic, J. Zaanen, and K. Schalm, “Fermions and the AdS/CFT correspondence: quantum phase transitions and the emergent Fermi-liquid,” [0904.1993](#).
- [10] T. Faulkner, H. Liu, J. McGreevy, and D. Vegh, “Emergent quantum criticality, Fermi surfaces, and AdS₂,” [0907.2694](#).
- [11] M. Rozali and L. Brits, “Holography and Fermions at a Finite Chemical Potential,” *Can. J. Phys.* **87** (2009) 271–277, [0810.5321](#).
- [12] L. J. Romans, “Supersymmetric, cold and lukewarm black holes in cosmological Einstein-Maxwell theory,” *Nucl. Phys.* **B383** (1992) 395–415, [hep-th/9203018](#).
- [13] N. Iqbal and H. Liu, “Real-time response in AdS/CFT with application to spinors,” [0903.2596](#).
- [14] T. Albash and C. V. Johnson, “Landau Levels, Magnetic Fields and Holographic Fermi Liquids,” [1001.3700](#).